NANO LETTERS

LETTER

pubs.acs.org/NanoLett

Ethylene Irradiation: A New Route to Grow Graphene on Low Reactivity Metals

Antonio J. Martínez-Galera,* Iván Brihuega, and José M. Gómez-Rodríguez

Departamento de Física de la Materia Condensada, C-III, Universidad Autónoma de Madrid, E-28049, Madrid, Spain

Supporting Information

ABSTRACT:

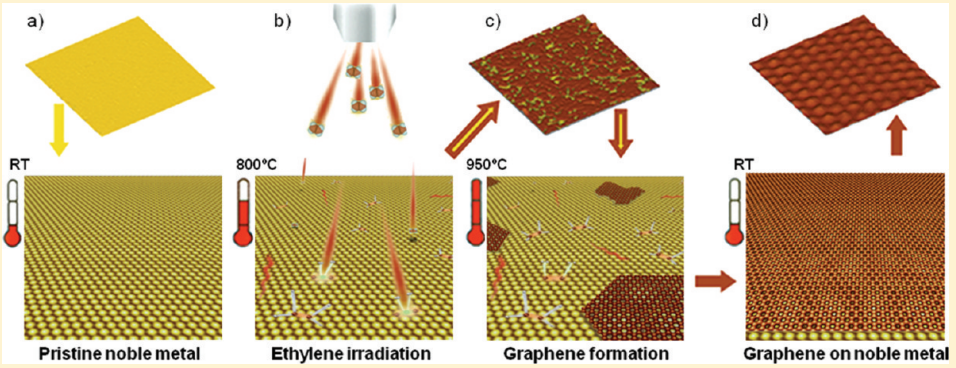

A novel technique for growing graphene on relatively inert metals, consisting in the thermal decomposition of low energy ethylene ions irradiated on hot metal surfaces in ultrahigh vacuum, is reported. By this route, we have grown graphene monolayers on Cu(111) and, for the first time, on Au(111) surfaces. For both noble metal substrates, but particularly for Au(111), our scanning tunneling microscopy and spectroscopy measurements provide sound evidence of a very weak graphene−metal interaction.

KEYWORDS: Graphene, irradiation by ethylene, Cu(111), Au(111), scanning tunneling microscopy

Graphene, a single layer of carbon atoms with the same arrangement as that in the graphite basal plane, has attracted remarkable interest in the scientific community as a straightforward consequence of the first experimental observation of some of its fascinating properties, which became a reality in 2004.[1] The key to this advance resided in the development of a technique for producing graphene consisting in the micromechanical cleavage of graphite and the subsequent transfer of the exfoliated graphene flakes onto SiO_2 substrates. Although very valuable for research purposes, this route is not efficient enough to provide the large amounts of graphene that would be needed for industrial applications. Currently, several alternatives are being intensively studied with the main aim of achieving a method of producing high-quality graphene films with controllable thickness in order to allow its implementation in future devices. One alternative attempted is the reduction of graphene oxide flakes,[2] but it produces graphene with reduced mobility of the charge carriers. The graphitization of silicon carbide (SiC) substrates, although it has served as a platform for the observation of some exciting properties of graphene,[3,4] presents the inconvenience that it is not easy to detach the graphene sheet from the SiC substrate. Graphene epitaxially grown onto metals gives rise to high-quality graphene films,[5−8] and these days it is considered as one of the most promising approaches since chemical etching of the metal and transfer of the graphene film onto arbitrary substrates have been achieved.[9,10] In addition, the growth of graphene on metals provides a model system for studying the properties of the contact between graphene and metal,[11,12] a key issue both from a fundamental point of view and also to allow the integration of graphene in real devices. As a consequence, huge efforts are being made to develop new methods of obtaining graphene films on metals.[13−16] The most commonly employed techniques are segregation of carbon atoms from the bulk of the metal[7,8] and thermal decomposition of hydrocarbons catalyzed via its adsorption on the surface of the metal.[5,6,10] In contrast with hydrocarbon decomposition, where graphene growth is mainly self-limited to monolayers,[10] graphene multilayers have been frequently found by segregation and could give rise to problems in achieving a monolayer.[9,17] The hydrocarbon decomposition can be performed in two ways: the adsorption of the hydrocarbons on the metal surface before annealing at high temperatures,[18,19] and chemical vapor deposition (CVD).[5,9,10] While by means of CVD and under different pressure conditions including ultrahigh vacuum (UHV) it is possible to obtain high coverages of single layer graphene, the preadsorption of hydrocarbons followed by annealing usually gives rise to scattered graphene islands partially covering the metal surface.[19]

Therefore, CVD is a powerful technique to produce large graphene flakes of high quality over a great variety of metals and, at the moment, it is the only method suitable for large-scale production of high-quality graphene films with uniform thickness.[10,20] However,

Received: April 15, 2011
Revised: June 22, 2011
Published: August 08, 2011

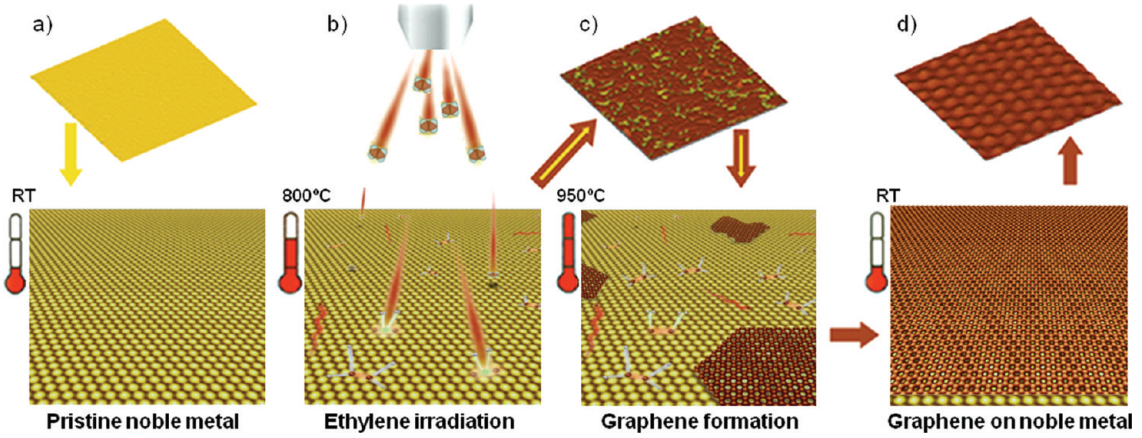

Figure 1. Schematic drawing of the new method of growing graphene on low reactivity metals: (a) clean metal surface; (b) low energy ethylene irradiation on the metal at high temperatures; (c) further annealing at higher temperatures; (d) graphene layer epitaxially grown on the metal surface. The upper part of the figure shows 50 × 50 nm^2 STM images acquired during the growth of graphene on Cu(111) after each preparation step, as indicated by the arrows. Yellow regions correspond to the Cu(111) surface, while the red regions correspond to carbon areas. Tunneling parameters: (a) I_T = 1 nA, V_s = 60 mV; (b) I_T = 0.2 nA, V_s = 745 mV; (c) I_T = 19 nA, V_s = 280 mV.

due to the catalytic role of the metal surface, it could fail with some low reactivity metals where the hydrocarbons are hardly adsorbed. Here, we present a novel route, complementary to CVD, which can be used with relatively inert metals. We demonstrate its applicability by growing single graphene layers onto Cu(111) and even on Au(111), a quite inert surface where graphene had not been grown until now. Thus, our new method paves the way to extend the range of possible substrates for the epitaxial growth of graphene to other low reactivity metals. This work has been performed in UHV and using single crystals as metal substrates for the graphene growth in order to characterize it at the atomic scale by scanning tunneling microscopy (STM).

The technique we present for growing graphene onto low reactivity metals consists in the thermal decomposition of fragments of hydrocarbons produced by irradiating the surface of the metal, maintained at high temperatures, with an ion beam resulting from the electron bombardment of ethylene (Figure 1). The irradiation has been performed by means of an ion gun where ethylene is ionized by electron impact and the resulting ion beam is accelerated against the hot surface of the metal. It has been reported that after the ionization of ethylene by electron impact, the ion beam consists mainly of $C_2H_4^+$ ions, but smaller ions such as $C_2H_3^+$, $C_2H_2^+$, C_2H^+, CH_2^+, and CH^+ with decreasing concentrations could also be present.[21] Once the ions of the beam reach the metal surface, they might be neutralized or dissociated into smaller fragments. The adsorption on the surface and the subsequent decomposition of this carbon-containing species have been reported to be enhanced compared to the case of thermal deposition of ethylene.[22,23] However, at the ion beam energies employed here (see below), the possibility of implantation of ethylene ions and/or smaller fragments in the first subsurface layers is not ruled out. Thermal decomposition of such hydrocarbon fragments might also produce hydrogen desorption and diffusion of carbon to the surface. Anyway, under further annealing at higher temperatures once the irradiation is stopped, the result is the formation of a graphene layer onto the metal surface. The best results for the graphene growth over both Cu(111) and Au(111) substrates were obtained by keeping the previously cleaned substrate at temperatures of approximately 800 °C during the irradiation with ions of 500 eV. After the irradiation, the sample is further annealed at around 900−950 °C for 10 min (for further details about the method see Supporting Information). Overfilling the UHV chamber with ethylene at high pressures of 4×10^{-4} Torr was necessary to obtain typical currents of the accelerated ions between 1 and 2 μA. Further annealing was applied after the irradiation process. Different graphene coverages were obtained (between 0.2 and 1 ML) on both Cu(111) and Au(111), by fine-tuning the irradiation time and current as well as the annealing time. Typically, to obtain a final graphene coverage of 0.9 ML on Cu(111) or 0.5 ML on Au(111), 35 min of irradiation at 1.8 μA followed by 10 min of further annealing were required. However, adsorption and decomposition of ethylene by thermal deposition on the surface were negligible even at such high pressures. To demonstrate this, we exposed the hot metal surface under the same conditions of temperature and ethylene pressure during 60 min but with the ion gun turned off. In this case, no carbon was detected on the metal surface in our Auger spectroscopy measurements (see Figure S2, Supporting Information).

Using the above-described procedure on a Cu(111) substrate, we have obtained high-quality graphene single layers. Such quality has been atomically characterized in UHV by using a home-built variable temperature scanning tunneling microscope (VT-STM)[24] and WSxM software.[25] Figure 2a displays an STM image of an area of 93 nm × 93 nm, where an atomically perfect graphene flake with a moiré pattern of approximately 6.3 nm is observed. Several moiré patterns with different periodicities have been detected in the present experiments, as would be expected for graphene monolayers weakly coupled to the metal substrate. As an example, panels b and c of Figure 2 show atomically resolved STM images of two of the most frequently found moiré patterns. The moiré pattern observed in Figure 2b is the same as that shown in Figure 2a and can be explained by a small rotation (0.8°) of the graphene layer with respect to the Cu(111) substrate and a mismatch of the graphene lattice of 0.2%. The moiré pattern displayed in Figure 2c exhibits a periodicity of around 2 nm that can be explained by a rotation of 7° and a mismatch of 0.7% (see Supporting Information).

The versatility of the method presented here is demonstrated by growing, for the first time, monolayer graphene on Au(111) surfaces. Figure 3a shows an STM image acquired over an area of 53 nm × 41 nm exhibiting several graphene flakes (in red) over the Au(111) substrate (in yellow). The herringbone reconstruction

dx.doi.org/10.1021/nl201281m |*Nano Lett.* 2011, 11, 3576–3580

characteristic of clean Au(111) can be resolved on the bare area. On the graphene flakes, reasonably large defect-free graphene regions exhibiting a symmetric honeycomb structure with the periodicity of graphene as expected for ML graphene on a weakly interacting substrate[26] are routinely found (Figure 3b). On the large scale, the degree of perfection is not as high as in the case of Cu(111) surfaces and some defects (white spots) are also seen. Most of them could be nanobubbles and/or the beginning of wrinkle formation, similar to those observed in graphene grown on other metals such as Pt(111)[27,28] or Ir(111),[28] originated in the graphene layer due to the mismatch in the graphene thermal expansion coefficient with respect to the substrate one. We have also performed LEED measurements and Auger spectroscopy (Figure 3c,d) that confirm the formation of an ordered carbon layer on top of the Au(111) substrate on the macroscopic scale. Several orientations of the graphene layer with respect to the substrate can be deduced from both high-resolution STM images and LEED patterns. In particular, rotations between the graphene layer and Au(111) of close to 3° and 25° can be observed (see Figure 3c and Supporting Information).

Our success in growing epitaxial graphene over Cu(111) and Au(111) surfaces has served us as a platform for investigating the properties of the graphene−metal contact for both systems. Our experimental results show that for both Cu and Au the interaction with the substrate is very weak, probably weaker than in any other reported graphene/metal system. A first evidence is shown in Figure 4a, which presents an STM image measured at low temperature (40 K) on a graphene monolayer grown on Cu(111) with a point defect in its middle. Surrounding the defect, a remarkable distortion of the graphene lattice with a $(\sqrt{3} \times \sqrt{3})R30°$ (R3 in the following) periodicity can be observed. Such R3 modulations of the local density of states (LDOS) are expected for ideal graphene in the presence of a point defect as the result of the intervalley scattering processes generated around it.[29] In well-decoupled graphene layers, such as epitaxial graphene on SiC or HOPG surfaces, large R3 patterns associated with atomic-size impurities have been observed by means of low-bias STM images, which are a measure of the LDOS at E_F.[4,29−34] Therefore, in analogy with the conclusions drawn from those systems, the existence of well extended R3 patterns, observed here in our STM images around point defects on epitaxial graphene not only on Cu(111) but also on Au(111) (not shown) can be explained as a direct consequence of the weak coupling between graphene and metal for both Cu(111) and Au(111) substrates.

Additional support for this weak interaction can be obtained through the observation, by means of low-bias STM images such as the one shown in Figure 4b, of standing waves patterns through the graphene layer. In these kinds of images, standing wave patterns such as those resulting from the quantum interference of electrons on surface states of pristine metal surfaces can be resolved. Surface states of noble metals through adsorbed single layers have also been observed upon adsorption of low-interacting materials such as rare-gas atoms,[35] insulating NaCl,[36] or aromatic molecules.[37,38] In all these cases, due to the small existing interaction, the surface state band of the original substrate is only slightly perturbed as reflected by minor changes in the Fermi wavevector (k_F). We have estimated k_F from the present experiments by Fourier transforming low-bias images such as the one shown in Figure 4b. For graphene grown on Cu(111), the measured value, $k_F = 0.18 \pm 0.03$ Å^{-1}, is somehow smaller than that expected (0.215 Å^{-1}) for the pristine Cu(111) surface,[39] suggesting a slight upward shift of the surface state band if the effective mass is conserved.[40] Such a small upward shift could also contribute to the downward shift of the Dirac

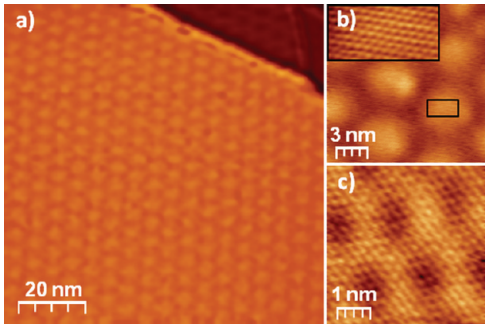

Figure 2. (a) STM image acquired over an area of 93 nm × 93 nm of a high-quality graphene sheet epitaxially grown on Cu(111) exhibiting a moiré pattern with 6.3 nm periodicity. Tunneling parameters: $V_s = 110$ mV, $I_t = 21$ nA. (b, c) STM images with atomic resolution recorded on areas of 15 × 15 nm^2 and 4.6 × 4.6 nm^2, respectively, of two of the most frequently found moiré patterns. Tunneling parameters: (b) $V_s = 80$ mV, $I_t = 21$ nA and (c) $V_s = 50$ mV, $I_t = 22$ nA. The inset in (b) is a zoom-in corresponding to the 3.0 nm × 1.4 nm area marked with a black rectangle.

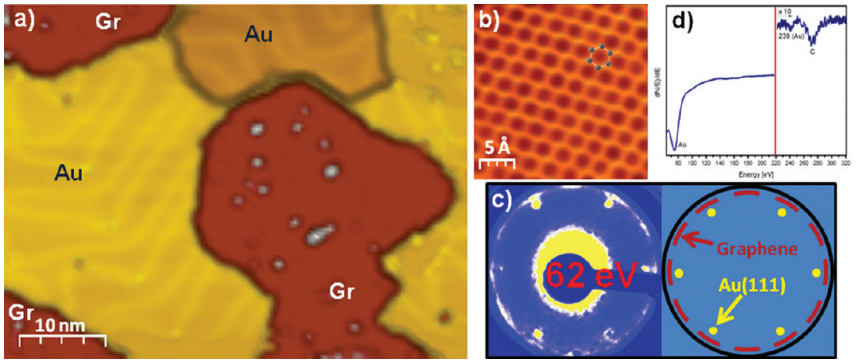

Figure 3. (a) STM image of an area of 53 × 41 nm^2 exhibiting three graphene flakes grown epitaxially on a Au(111) surface. The herringbone reconstruction characteristic of the Au(111) surface can be observed. Tunneling parameters: $V_s = 500$ mV, $I_t = 0.5$ nA. (b) STM image over a defect-free graphene area displaying the honeycomb structure. Tunneling parameters: $V_s = 30$ mV, $I_t = 21$ nA; size: 2.5 × 2.5 nm^2. (c) LEED pattern acquired at 62 eV on a graphene/Au(111) sample together with a schematic drawing to facilitate its understanding. Segments with atomic periodicity corresponding to the graphene lattice located around ±3° and ±25° are visible (red lines) together with the (1 × 1) spots corresponding to the Au(111) substrate (yellow dots). (d) AES spectrum of the graphene layer grown epitaxially on Au(111). The energy of the primary beam was 2.8 keV.

dx.doi.org/10.1021/nl201281m |*Nano Lett.* 2011, 11, 3576–3580

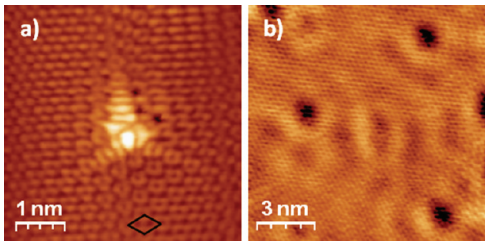

Figure 4. (a) STM image with atomic resolution measured at 40 K on a region of graphene/Cu(111), where a point defect as well as the R3 pattern arising from intervalley scattering in the graphene layer is observed. The R3 unit cell of the scattering pattern is outlined in black. Such R3 modulations are also visible by Fourier transforming this image, as shown in the Supporting Information. Tunneling parameters: V_s = 100 mV, I_t = 0.2 nA; size: 4.7 × 4.7 nm^2. (b) Atomically resolved STM image acquired at 40 K on top of a graphene flake. The standing wave patterns corresponding to the scattering of the surface state electrons of the underlying Cu(111) substrate are observed through the graphene layer. Tunneling parameters: V_s = 60 mV, I_t = 2.7 nA; size: 12 × 12 nm^2.

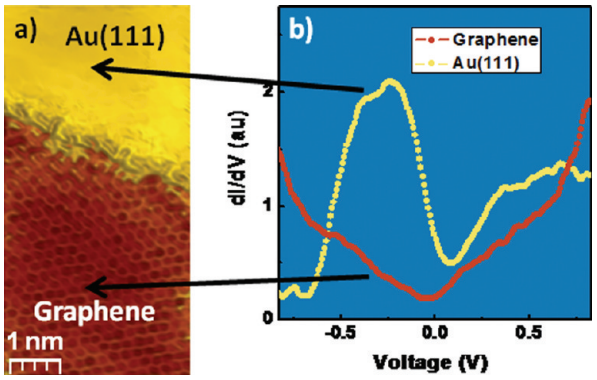

Figure 5. (a) STM image measured on graphene/Au(111) showing the interface between a graphene flake and a narrow Au(111) terrace. Tunneling parameters: V_s = 200 mV, I_t = 11 nA. Image size: 3.7 × 7.3 nm^2. (b) Room temperature differential conductance plots (dI/dV vs V) obtained by mathematical differentiation of I/V curves consecutively performed at the positions indicated by the arrows on the clean Au(111) and on the graphene/Au(111) regions displayed on (a).

point reported for graphene on Cu(111).[6] Moreover, high-resolution images such as the one shown in Figure 4b reveal that the standing wave patterns related to the Cu(111) substrate can be imaged at the same time as the atomic periodicity of the graphene layer above it. This is an important observation as it shows that most of the defects present in the underlying Cu(111) surface, which give rise to the standing wave interference patterns on the metal surface, do not act as scattering centers for the quasiparticles belonging to the graphene layer, since an R3 pattern is not observed around them. Such R3 patterns are a signature of intervalley scattering processes, which play a key role in the transport properties of graphene systems, and therefore their absence implies that these defects in the Cu(111) metal substrate are not expected to strongly affect the mobility of the charge carriers of the graphene layer.

The growth of graphene on an atomically controlled Au(111) surface has allowed us, for the first time, to electronically characterize the properties of the graphene/Au interface on a well-known surface, a fundamental step to understand and optimize the contact properties of graphene with such a commonly used material in graphene contacts. For Au(111) substrates, we have also observed standing wave patterns through the graphene layer. In this case, the Fermi wave vector estimated from STM images measured at low bias is $k_F = 0.17 \pm 0.01$ Å^{-1} (see Figure S8, Supporting Information). This value is in perfect agreement with $k_F = 0.167$ Å^{-1} for the surface state of the pristine Au(111) surface,[39] suggesting that significant changes are not expected in the energy onset of the Au surface state band or in the energy position of the Dirac point. Further insight into the electronic structure of graphene on Au(111) has been gained by scanning tunneling spectroscopy (STS). Figure 5b shows differential conductance plots (dI/dV vs V) consecutively measured at room temperature (RT) with the same microscopic tip both on the pristine Au(111) surface and on graphene. The reference spectrum, measured on the relatively narrow Au(111) terrace shown in Figure 5a (yellow dots), exhibits the expected rise in the LDOS associated with the Au(111) surface state onset at around −0.5 eV, which ensures tip quality. A broad dip at positive voltages can also be observed due to the electronic confinement inside the terrace. The spectrum measured on the graphene region (red line in Figure 5b) exhibits the characteristic V shape of free-standing graphene with a minimum very close to the Fermi level. We have reproducibly performed this kind of STS measurement with many different tips and sample preparations; see for example Figure S10 (Supporting Information) where we show a new pair of dI/dV curves measured at 40 K on a large Au(111) terrace, together with a dI/dV spectra measured, with the same tip, on a graphene region. All our dI/dV curves on top of graphene layers were consistent with the ones plotted in red in Figure 5b and Figure S10 (Supporting Information), showing a LDOS with minimum at $\sim E_F$ accompanied by a fairly linear increase as expected for free-standing graphene. Therefore, all our data suggest that this minimum can be associated to the Dirac point of graphene's electronic structure, indicating that no appreciable doping exists for this remarkable system. This is the first experimental measurement of the Dirac point position for monolayer graphene grown epitaxially on Au(111) surfaces and again points to extremely low interaction of the graphene with the underlying Au(111) surface. This result is in good agreement with theoretical calculations, which predict small shifts of the Dirac point with respect to the Fermi level,[11,41−44] and with experimental measurements performed by angle-resolved photoemission spectroscopy for graphene grown onto Ru(111),[45] Ni(111),[46,47] and SiC[48] substrates, which show that it is possible to electronically decouple graphene from the substrate by intercalating the appropriate amount of Au.

In summary, we have developed a new technique for growing epitaxial graphene which can be used as an alternative to CVD onto low reactivity metals where hydrocarbons are hardly adsorbed. It consists in the thermal decomposition of hydrocarbon fragments produced by irradiation of the metal surface at high temperature with low-energy ethylene ions. This route has allowed high-quality graphene to be grown not only on Cu(111) but also, for the first time, on Au(111). This has given us the opportunity to obtain by STM the first experimental measure of the Dirac point on an atomically characterized Au substrate. In addition, we have observed by STM, through the graphene layer, the standing waves originating from the scattering of surface state electrons on Cu(111) and Au(111). The comparison between the wave vector found for such standing waves and the Fermi wave vector of the pristine surfaces together with the observation

of R3 patterns on the graphene layers with large decay lengths is in good agreement with the picture of a very weak graphene−metal interaction for both substrates. In the case of Au(111), such interaction appears to be exceptionally weak.

■ ASSOCIATED CONTENT

Supporting Information. Additional information about the preparation method, STM and STS measurements, and LEED and Auger spectroscopy data and further details about the rotation angles between graphene and the substrate and regarding the observation of standing waves through the graphene layer for both metals. This material is available free of charge via the Internet at http://pubs.acs.org.

■ AUTHOR INFORMATION

Corresponding Author
*E-mail: antonio.galera@uam.es.

■ ACKNOWLEDGMENT

Financial support from the Comunidad de Madrid, under Contract Nos. CPI/0256/2007 and S2009/MAT-1467, and from the Spanish Ministerio de Ciencia e Innovación under Grant Nos. MAT2010-14902 and CSD2010-00024 is gratefully acknowledged. I.B. was supported by the Ramón y Cajal program.

■ REFERENCES

(1) Novoselov, K. S.; Geim, A. K.; Morozov, S. V.; Jiang, D.; Zhang, Y.; Dubonos, S. V.; Grigorieva, I. V.; Firsov, A. A. *Science* **2004**, *306*, 666.
(2) Gómez-Navarro, C.; Weitz, R. T.; Bittner, A. M.; Scolari, M.; Mews, A.; Burghard, M.; Kern, K. *Nano Lett.* **2007**, *7*, 3499.
(3) Berger, C.; Song, Z. M.; Li, T. B.; Li, X. B.; Ogbazghi, A. Y.; Feng, R.; Dai, Z. T.; Marchenkov, A. N.; Conrad, E. H.; First, P. N.; de Heer, W. A. *J. Phys. Chem. B* **2004**, *108*, 19912.
(4) Brihuega, I.; Mallet, P.; Bena, C.; Bose, S.; Michaelis, C.; Vitali, L.; Varchon, F.; Magaud, L.; Kern, K.; Veuillen, J.-Y. *Phys. Rev. Lett.* **2008**, *101*, 206802.
(5) Coraux, J.; N'Diaye, A. T.; Busse, C.; Michely, T. *Nano Lett.* **2008**, *8*, 565.
(6) Gao, L.; Guest, J. R.; Guisinger, N. P. *Nano Lett.* **2010**, *10*, 3512.
(7) Marchini, S.; Günther, S.; Wintterlin, J. *Phys. Rev. B* **2007**, *76*, 075429.
(8) Sutter, P.; Sadowski, J. T.; Sutter, E. *Phys. Rev. B* **2009**, *80*, 245411.
(9) Reina, A.; Jia, X.; Ho, J.; Nezich, D.; Son, H.; Bulovic, V.; Dresselhaus, M. S.; Kong, J. *Nano Lett.* **2009**, *9*, 30.
(10) Li, X.; Cai, W.; An, J.; Kim, S.; Nah, J.; Yang, D.; Piner, R.; Velamakanni, A.; Jung, I.; Tutuc, E.; Banerjee, S. K.; Colombo, L.; Ruoff, R. S. *Science* **2009**, *324*, 1312.
(11) Giovannetti, G.; Khomyakov, P. A.; Brocks, G.; Karpan, V. M.; van den Brink, J.; Kelly, P. J. *Phys. Rev. Lett.* **2008**, *101*, 026803.
(12) Preobrajenski, A. B.; Ng, M. L.; Vinogradov, A. S.; Mårtensson, N. *Phys. Rev B* **2008**, *78*, 073401.
(13) Liu, N.; Fu, L.; Dai, B.; Yan, K.; Liu, X.; Zhao, R.; Zhang, Y.; Liu, Z. *Nano Lett.* **2011**, *11*, 297.
(14) Amini, S.; Garay, J.; Liu, G.; Balandin, A. A.; Abbaschian, R. *J. Appl. Phys.* **2010**, *108*, 094321.
(15) Garaj, S.; Hubbard, W.; Golovchenko, J. A. *Appl. Phys. Lett.* **2010**, *97*, 183103.
(16) Otero, G.; González, C.; Pinardi, A. L.; Merino, P.; Gardonio, S.; Lizzit, S.; Blanco-Rey, M.; Van de Rui,t, K.; Flipse, C. F. J.; Méndez, J.; de Andrés, P. L.; Martín-Gago, J. A. *Phys. Rev. Lett.* **2010**, *105*, 216102.
(17) Cao, H.; Yu, Q.; Colby, R.; Pandey, D.; Park, C. S.; Lian, J.; Zemlyanov, D.; Childres, I.; Drachev, V.; Stach, E. A.; Hussain, M.; Li, H.; Pei, S. S.; Chen, Y. P. *J. Appl. Phys.* **2010**, *107*, 044310.
(18) Enachescu, M.; Schleef, D.; Ogletree, D. F.; Salmeron, M. *Phys. Rev. B* **1999**, *60*, 16913.
(19) N'Diaye, A. T.; Coraux, J.; Plasa, T. N.; Busse, C.; Michely, T. *New J. Phys.* **2008**, *10*, 043033.
(20) Kim, K. S.; Zhao, Y.; Jang, H.; Lee, S. Y.; Kim, J. M.; Kim, K. S.; Ahn, J. H.; Kim, P.; Choi, J. Y.; Hong, B. H. *Nature* **2009**, *457*, 706.
(21) Tian, C.; Vidal, C. R. *Chem. Phys. Lett.* **1998**, *288*, 499.
(22) Yu, H.; Leung, K. T. *Surf. Sci.* **1998**, *401*, 269.
(23) Yu, H.; Leung, K. T. *Surf. Sci.* **1999**, *432*, 245.
(24) Custance, O.; Brochard, S.; Brihuega, I.; Artacho, E.; Soler, J. M.; Baró, A. M.; Gómez-Rodríguez, J. M. *Phys. Rev. B* **2003**, *67*, 235410.
(25) Horcas, I.; Fernández, R.; Gómez-Rodríguez, J. M.; Colchero, J.; Gómez-Herrero, J.; Baro, A. M. *Rev. Sci. Instrum.* **2007**, *78*, 013705.
(26) Stolyarova, E.; Rim, K. T.; Ryu, S. M.; Maultzsch, J.; Kim, P.; Brus, L. E.; Heinz, T. F.; Hybertsen, M. S.; Flynn, G. W. *Proc. Natl. Acad. Sci. U.S.A.* **2007**, *104*, 9209.
(27) Levy, N.; Burke, S. A.; Meaker, K. L.; Panlasigui, M.; Zettl, A.; Guinea, F.; Castro Neto, A. H.; Crommie, M. F. *Science* **2010**, *329*, 544.
(28) N'Diaye, A. T.; van Gastel, R.; Martinez-Galera, A. J.; Coraux, J.; Hattab, H.; Wall, D.; ZU Heringdorf, F. J. M.; Horn-von Hoegen, M.; Gomez-Rodriguez, J. M.; Poelsema, B.; Busse, C.; Michely, T. *New J. Phys.* **2009**, *11*, 113056.
(29) Mallet, P.; Varchon, F.; Naud, C.; Magaud, L.; Berger, C.; Veuillen, J.-Y. *Phys. Rev. B* **2007**, *76*, 041403(R).
(30) Mizes, H. A.; Foster, J. S. *Science* **1989**, *244*, 559.
(31) Kelly, K. F.; Sarkar, D.; Hale, G. D.; Oldenburg, S. J.; Halas, N. J. *Science* **1996**, *273*, 1371.
(32) Ruffieux, P.; Gröning, O.; Schwaller, P.; Schlapbach, L.; Gröning, P. *Phys. Rev. Lett.* **2000**, *84*, 4910.
(33) Rutter, G. M.; Crain, J. N.; Guisinger, N. P.; Li, T.; First, P. N.; Stroscio, J. A. *Science* **2007**, *317*, 219.
(34) Ugeda, M. M.; Brihuega, I.; Guinea, F.; Gómez-Rodríguez, J. M. *Phys. Rev. Lett.* **2010**, *104*, 096804.
(35) Andreev, T.; Barke, I.; Hövel, H. *Phys. Rev. B* **2004**, *70*, 205426.
(36) Repp, J.; Meyer, G.; Rieder, K.-H. *Phys. Rev. Lett.* **2004**, *92*, 036803.
(37) Nicoara, N.; Román, E.; Gómez-Rodríguez, J. M.; Martín-Gago, J. A.; Méndez, J. *Org. Electron.* **2006**, *7*, 287.
(38) Ziroff, J.; Gold, P.; Bendounan, A.; Forster, F.; Reinert, F. *Surf. Sci.* **2009**, *603*, 354.
(39) Reinert, F.; Nicolay, G.; Schmidt, S.; Ehm, D.; Hüfner, S. *Phys. Rev. B* **2001**, *63*, 115415.
(40) Jeon, I.; Yang, H.; Lee, S. H.; Heo, J.; Seo, D. H.; Shin, J.; Chung, U. I.; Kim, Z. G.; Chung, H. J.; Seo, S. *ACS Nano* **2011**, *5*, 1915.
(41) Khomyakov, P. A.; Giovannetti, G.; Rusu, P. C.; Brocks, G.; van den Brink, J.; Kelly, P. J. *Phys. Rev. B* **2009**, *79*, 195425.
(42) Hamada, I.; Otani, M. *Phys. Rev. B* **2010**, *82*, 153412.
(43) Vanin, M.; Mortensen, J. J.; Kelkkanen, A. K.; Garcia-Lastra, J. M.; Thygesen, K. S.; Jacobsen, K. W. *Phys. Rev. B* **2010**, *81*, 081408.
(44) Sławińska, J.; Dabrowski P.; Zasada I. arXiv:1102.4543v1.
(45) Enderlein, C.; Kim, Y. S.; Bostwick, A.; Rotenberg, E.; Horn, K. *New J. Phys.* **2010**, *12*, 033014.
(46) Varykhalov, A.; Sánchez-Barriga, J.; Shikin, A. M.; Biswas, C.; Vescovo, E.; Rybkin, A.; Marchenko, D.; Rader, O. *Phys. Rev. Lett.* **2008**, *101*, 157601.
(47) Varykhalov, A.; Scholz, M. R.; Kim, T. K.; Rader, O. *Phys. Rev. B* **2010**, *82*, 121101.
(48) Gierz, I.; Suzuki, T.; Weitz, R. T.; Lee, D. S.; Krauss, B.; Riedl, C.; Starke, U.; Höchst, H.; Smet, J. H.; Ast, C. R.; Kern, K. *Phys. Rev. B* **2010**, *81*, 235408.